Void evolution in tungsten and tungsten-5wt.% tantalum under in-situ proton irradiation at 800 and 1000°C

Ipatova, I.; Harrison, R.W.; Donnelly, S.E.; Rushton, M.J.D.; Middleburgh, S.C.; Jimenez-Melero, E.

Journal of Nuclear Materials

Published: 01/12/2019

Peer reviewed version

Void evolution in tungsten and tungsten-5wt.% tantalum under in-situ proton irradiation at 800 and 1000 °C

I. Ipatova[a*], R.W. Harrison[b,c], S. E. Donnelly[b], M.J.D. Rushton[a], S.C. Middleburgh[a], E. Jimenez-Melero[d]

[a]*Nuclear Futures Institute, Bangor University, Dean Street, Bangor Gwynedd, LL57 1 UT, UK*

[b]*School of Computing and Engineering, University of Huddersfield, Huddersfield, HD1 3DH, UK*

[c]*School of Mechanical, Aerospace and Civil Engineering, Materials Performance Centre, The University of Manchester, Manchester M13 9PL, UK*

[d]*Materials Performance Centre, School of Materials, The University of Manchester, Manchester M13 9PL, UK*

Corresponding author (*):

Nuclear Futures Institute

Bangor University

Dean Street

Bangor, Gwynedd

LL57 1UT

United Kingdom

Tel.: +44 7849290480

Email: i.ipatova@bangor.ac.uk

Abstract

We have probed void evolution in polycrystalline W and W-5wt.%Ta material at 800 and 1000 °C, by transmission electron microscopy during in-situ irradiation with a 40 keV proton beam. The presence of radiation-induced dislocation loops was not observed prior to void formation at those elevated temperatures. The damaged W microstructure was characterised by the presence of a population of randomly distributed voids, whose number density reduces when the irradiation temperature increases. Soft impingement of voids becomes noticeable at damage levels ≥0.2 dpa. In contrast, the excess of free vacancies in the W-5wt.%Ta material irradiated at 800 °C only leads to the formation of visible voids in this TEM study (≥2 nm) after post-irradiation annealing of the sample at 1000 °C. Solute Ta atoms also cause a significant increase in the number density of voids when comparing the microstructure of both materials irradiated at 1000 °C, and a gradual progression towards saturation in average void size at ≥0.2 dpa. Moreover, we have detected a progressive transition from a spherical to a faceted shape in a number of voids present in both materials at damage levels ≥0.3 dpa.

Keywords: refractory metals, materials for fusion, radiation damage, faceted voids, transmission electron microscopy

1. Introduction

Tungsten has traditionally stood out within the refractory metal group as the prime plasma-facing candidate for armour components of magnetically-confined tokamak fusion reactors. Tungsten may potentially be used in the future, for the underlying cooling structures as well, if taking advantage of the incipient additive manufacturing technologies for optimised geometries [1, 2]. The attractiveness of tungsten is due to its high melting point (T_m=3422 °C) and its resistance to sputtering from accidental plasma-material interactions, together with suitable thermal conductivity, shock resistance and high-temperature strength [3-5]. Tungsten was used as a ~25 μm-thick coating on the carbon fibre composite divertor tiles during the second JET ITER-like wall campaign of 2013–2014 [6, 7]. In ITER, tungsten tiles will also be placed on the top section of the arched stainless-steel plasma confinement construction. During regular operation modes, the full-tungsten armour will experience heat loads of ~6.5-10 MW/m^2, attaining values close to 20 MW/m^2 during short transient events. Additionally, a 14 MeV neutron-induced damage level of ~0.1 dpa is predicted to be accumulated by the tungsten monoblocks after the 4-year ITER nuclear phase prior to the cassette replacement of the first divertor, and ~0.5 dpa for permanent divertor components during ITER's end-of-life operation [8]. Furthermore, current blanket designs for the future fusion demonstration power plant (DEMO) are based on a first wall in which the tungsten armour is joined to a structure made of Reduced Activation Ferritic Martensitic (RAFM) steel [9]. Water-cooled DEMO divertor designs under consideration are also based on ITER-like tungsten monoblocks [10].

The recommended low-temperature limit for safe operation of body-centred cubic (bcc) metals such as tungsten is dictated by radiation-induced hardening and embrittlement, occurring even for doses ≤1 dpa [11]. Unfortunately, tungsten is inherently brittle at low temperatures, being characterized by a ductile-to-brittle transition temperature (DBTT) in the

range of ~200-400 °C. Both the value of the DBTT and of the low-temperature fracture toughness depend on the material processing route [12], and consequently on the microstructure and its anisotropy [13-15]. Additionally, exposure to neutron bombardment can shift the DBTT up to ~800-1000 °C and exacerbates the propensity for brittle failure at lower temperatures [11, 16, 17]. Tungsten irradiated with thermal or mixed neutrons to a damage level of <1 dpa and at temperatures below the vacancy-mediated stage III recovery, i.e. below ~0.15T_m depending on neutron energy spectrum and fluence, presents primarily a population of a_0/2<111> interstitial dislocation loops [18-20]. At higher temperatures, those loops tend to migrate and form larger interstitial-type structures [19]. Relatively high fast/mixed energy neutron fluences, at temperatures as low as 70 °C, also induce the occurrence of diffuse vacancy clusters and voids [21, 22]. Additionally, an increase in damage level to >1 dpa leads to the formation of nano-scale precipitates, involving Re and Os atoms resulting from transmutation [20]. These dominate radiation-induced hardening at relatively high damage levels [23]. Radiation-induced dislocation loops and voids act as effective trapping sites for mobile species and promote the nucleation of W-Re-Os precipitates [24]. In recent years ion irradiation experiments, especially those coupled with in-situ transmission electron microscopy, have shed complementary light on radiation-induced lattice defect evolution [25]. 1-D loop hopping has been observed in-situ in the temperature range of 300-700 °C, together with loop growth primarily by absorption [26, 27].

A promising strategy to make W more ductile is to introduce high-temperature elements (e.g. Ta, V, Ti, Mo, Re) either in solid solution or as short fibres in the W matrix [28-30]. In the former case, the predicted W-Ta phase diagram confirms that Ta remains in solid solution at concentrations <10wt.%Ta, whereas there is a tendency to form either B2 (CsCl-type) or DO_3 (Fe_3Al-type) ordered phases depending on temperature up to 727 °C and on Ta content >10wt.% [31]. Self-ion irradiation of W-5Ta (W-5wt%Ta) at 300-500 °C up to

33 dpa does not induce significant Ta clustering. However, the presence of 5wt.%Ta hinders the formation of radiation-induced Re-rich clusters, and also causes a higher dislocation loop density as compared to irradiated W under equivalent experimental conditions, but with a smaller average loop size [32-34]. Moreover, the loop size in W-5Ta proton-irradiated at 350 °C saturates at only 0.3 dpa, whereas the loop length in W continues to increase with damage level, giving rise to the formation of dislocation strings [35]. Recently systematic DFT simulations of tungsten self-interstitial atom clusters have revealed that Ta strongly repels interstitial clusters, especially when Ta is located on the periphery of the cluster [36].

In contrast, the upper temperature limit of structural materials such as W and its alloys is controlled by thermal creep, high-temperature helium embrittlement and void swelling [11]. In this respect, a significant number of annealing experiments have been reported in tungsten samples that had previously been irradiated at different low temperatures and damage levels, and with varying neutron energy spectra [20, 37-40], proton [41] or self-ion [27, 42] beams. Stage III recovery ($\geq 0.15T_m$) is characterised by vacancy migration, whereas in stage IV ($\geq 0.22T_m$) there is migration of vacancy clusters and vacancy-impurity complexes that become unstable and start emitting vacancies at $\geq 0.31T_m$ (stage V). The interstitial-type $a_0/2<111>$ dislocation loops emit self-interstitial atoms at temperatures >500 °C. The vacancy excess in the matrix evolves into vacancy-type $a_0/2<111>$ dislocation loops at 600-900 °C and into voids at >1000 °C [41]. Energy calculations of mesoscopic defect configurations in W using many-body interatomic potentials revealed that spherical voids are the most energetically favourable configuration, and vacancy-type loops therefore represent metastable configurations that would evolve into a void structure [43]. In neutron irradiated W, voids are already visible at ~430 °C, with a maximum in void swelling at $\sim 0.31Tm$ = 1060 °C [20, 44]. Voids larger than 10 nm were faceted, with facet planes of {211} and {110} [20]. A void lattice structure, characterised by a void lattice parameter of 195 Å and a

lattice parameter to average void size ratio of about six, was observed in neutron irradiated W at 550 °C to a neutron fluence of 1×10^{22} neutrons/cm^2 [45]. Moreover, a very low density of interstitial loops was detected in the temperature range of 500-800 °C up to 2.2 dpa [23]. Despite the wealth of reports about low-temperature radiation damage structures in W and alloys, their thermal stability post irradiation, and the formation of radiation-induced void structures in neutron irradiated W, the formation of defect structures in W at elevated temperatures and the role of Ta remain largely unexplored. In this study, we focus on in-situ monitoring of radiation-induced void evolution in W and W-5Ta at damage levels ≤0.4 dpa and at two target temperatures: 800 °C and 1000 °C.

2. Experimental

The initial W (99.95%) was provided by Goodfellow Cambridge Ltd. in the form of 1 mm thick sheet. The as-received W material was annealed in vacuum at 1400 °C for 2 h for recrystallization. The W-5Ta material was produced by powder metallurgy and provided by Plansee AG. The material was double forged and then annealed at 1600 °C for 1 h [46]. After delivery, the material was annealed for 1 h at 1000 °C for degassing [47]. Afterwards, smaller samples of 2×2cm^2 were cut and annealed at 1400 °C for 2 h to remove the defects from machining. TEM discs of both materials were prepared by mechanical pre-thinning, using SiC abrasive papers with successively smaller grit size (from grit 220 up to 4000). Then the procedure was followed by electropolishing at a temperature of ~ –5 °C using a Struers Tenupol-5 unit and an electrolyte comprising an aqueous solution of 0.5 wt% Na_2S for electropolishing W, or a mixture of 15 vol% sulphuric acid (95%) and 85 vol% methanol in the case of W-5Ta. The grain structure of both materials is presented in Fig. 1. The average grain size was 2.3 ± 0.7 mm (W-5Ta) and 3.9 ± 0.8 mm (W).

In-situ irradiation experiments were performed on the MIAMI-II TEM/ion accelerator system located at the University of Huddersfield [48]. The in-situ irradiation facility

comprises a Hitachi H-9500 transmission electron microscope (TEM) with a maximum operating voltage of 300 kV, coupled to a 350 kV National Electrostatics Corporation ion accelerator incorporating a Danfysik 921A ion source capable of providing ions of most species up to Au. The ion beam is incident on the sample at an angle of 18.7° to the electron beam. A double-tilt heating holder (Gatan Model 652) was used to reach the target temperature, i.e. 800 or 1000 °C. Equivalent TEM discs with an average thickness of ~100-110 nm, as determined by Convergent Electron Beam Diffraction (CBED) prior to the experiment, were irradiated with 40 keV protons at these two temperatures and at increasing damage levels up to 0.4 dpa for each material. The W-5Ta sample that had been irradiated, step-wise, up to 0.3 dpa at 800 °C was subsequently annealed at 1000 °C for 15 min. The main parameters for each irradiation experiment are collected in Table 1. The simulated damage profile was calculated using the SRIM software with the quick Kinchin-Pease approach [49, 50], using an average displacement energy of 90 eV [51] and default values for other software settings. The total current deposited on the sample is given in Table 1, and it was predicted that 97% of the incoming protons would have been transmitted through the foil. The Bragg peak for 40 keV protons in W occurs at 130 nm [35]. The reported damage levels correspond to the average values in the foil thickness. Micrographs were recorded along the zone axes <100> and <111> during the step-wise increase in damage level. The "out-of-focus" Fresnel imaging technique was used for bright-field void detection. Due to the inner potential difference between the void and the surrounding matrix, voids appear as white dots surrounded by black Fresnel fringes when recorded in an under-focused condition, and as dark dots with bright fringes in an over-focused condition. At each new damage level, a through-focal series of micrographs was taken with a defocus value $\Delta f \leq 1\mu m$ to feature voids of ≥1 nm in diameter [52]. The average void size was determined using the micrographs taken in over-focus condition and all voids visible in TEM were ≥2 nm.

3. Results

The occurrence and evolution of radiation-induced voids at the two selected temperatures are displayed in Fig. 2 and 3 for W and W-5Ta, respectively. The main microstructural parameters characterizing the void structure are collected in Table 2. In both materials and at both irradiation temperatures, the damaged structure was characterised by the formation of voids that changed in number, size and morphology with increasing damage level. The presence of radiation-induced dislocation loops was not detected at any of those irradiation temperatures. The number density of voids in the W sample irradiated at 800 °C increases continuously up to the maximum damage level of 0.4 dpa, with a faster increase up to 0.2 dpa, and a somewhat lower rate of change with damage level beyond 0.2 dpa. This transition coincides with a higher increase in the average void size with damage level at ≥0.2 dpa (Fig. 5). At the irradiation temperature of 1000 °C, W shows a similar trend in void evolution with damage level, but with a significantly lower density and a larger average void size. At 0.4 dpa, the void densities are $(52.5 \pm 5.3) \times 10^{21}$ m^{-3} (800 °C) and $(5.6 \pm 0.6) \times 10^{21}$ m^{-3} (1000 °C), whereas the average void sizes are 5.7 ± 0.6 nm (800 °C) and 7.1 ± 1.3 nm (1000 °C). In contrast, radiation-induced voids were not detected in the W-5Ta sample irradiated at 800 °C up to 0.3 dpa. Interestingly, voids are visible when the same sample is post-irradiation annealed at 1000 °C, with a void density of $4.9 \pm 1.4 \times 10^{21}$ m^{-3} and an average size of 4.9 ± 1.4 nm. This results from void agglomeration by a thermally activated process. Furthermore, the presence of 5wt.%Ta causes a significant increase in void density at 1000 °C as compared to the W sample irradiated at that temperature, from $5.6 \pm 0.6 \times 10^{21}$ m^{-3} (W) to $45.5 \pm 4.6 \times 10^{21}$ m^{-3} (W-5Ta) at 0.4 dpa. The average void size is comparable for both samples at 1000 °C and 0.4 dpa, namely 7.4 ± 0.9 nm (W) and 7.1 ± 1.3 nm (W-5Ta). However, the void size seems to gradually saturate at damage levels ≥0.2 dpa in W-5Ta, whereas it increases at a constant rate in W. Additionally, in both materials the voids

present in the microstructure gradually change their shape from spherical to either quadrilateral and/or hexagonal projections at ≥0.3 dpa at both irradiation temperatures – see insets in Fig. 2 & 3 and also Fig. 5. The size of the voids did not surpass 8 nm in either material, see Fig. 4.

4. Discussion

The irradiated microstructure at both 800 and 1000 °C is characterised by the presence of a relatively large number of voids, whose density and average size changes with damage level, irradiation temperature and Ta content. The radiation-induced voids seem, in general, to be uniformly and randomly distributed inside the matrix grains. However, we have also detected in some cases a fine denuded zone close to grain boundaries (see Fig. 2), and also a number of voids aligned along a pre-existing dislocation line in the material (e.g. see 0.1 dpa in Fig. 3). Grain boundaries tend to act as effective non-saturable sinks for radiation-induced point defects, leading to a local zone depleted of point defects that reduces markedly the nucleation and growth rate of vacancy clusters and voids [53, 54]. The $a_0/2$ <111>{1-10} edge dislocation–vacancy interaction in bcc metals is positive for vacancy locations above and below the dislocation slip plane [55]; the dislocation therefore assisting in the nucleation of voids in its vicinity. However, we have not detected the presence of radiation-induced dislocation loops at 800 or 1000 °C. At those elevated temperatures, interstitial dislocation loops would be unstable and emit self-interstitial atoms, or glide to the free sample surface [41]. The vacancy-type loops that would have formed at temperatures >600 °C, would transit into a more stable void configuration at temperatures close to 1000 °C [41]. Once reached a critical size, voids would continue growing by absorbing additional mobile vacancies from the matrix [56].

The population of voids present in irradiated W decreases in density when increasing the irradiation temperature from 800 to 1000 °C, whereas the average void size increases, in

agreement with previous work on neutron irradiated W samples to ~9.5 dpa that present a void swelling peak at $0.31T_m$ = 1060 °C [20, 44]. At damage levels ≥0.2 dpa, soft impingement starts to occur, so that voids have an enhanced probability of growing by absorption of free vacancies or void coalescence, as compared to the nucleation of additional voids. In contrast, the presence of 5wt.%Ta in solid solution precludes the formation of voids at 800 °C up to a damage level of 0.3 dpa. However, a significant excess of radiation-induced vacancies does exist in the microstructure, so that voids are detected when post-irradiation annealing the sample at 1000 °C for 15 min. First-principle calculations revealed that the Ta solute-vacancy interaction is attractive, with a binding energy of – 0.1 to – 0.3eV for the first-to-third nearest-neighbour positions [57]. This can be ascribed to the combination of, and competition between, electronic and strain-relief effects [57, 58]. The consequence is an effective vacancy trap nearby oversized Ta solute atoms [58], which leads to the hindrance at 800 °C of vacancy migration and void formation. Moreover, the average void size seems to gradually saturate at damage levels >0.2 dpa at the higher irradiation temperature of 1000 °C. At ≥0.3 dpa, the voids present in both materials transit steadily from spherical to faceted shapes, as dictated by the anisotropy of the surface energy and by the preferential absorption of diffusing vacancies on specific plane orientations with respect to the void surface [59]. At 1000 °C and 0.4 dpa, the number fraction of faceted voids amounts to 30% in W and only 12% in W-5Ta.

5. Conclusions

The in-situ TEM study of the microstructure evolution of W material proton-irradiated, step-wise up to an accumulated damage level of 0.4 dpa, revealed the presence of a population of voids that are in general randomly and uniformly distributed inside the grains of the matrix. An increase in irradiation temperature from 800 to 1000 °C causes a significant decrease in void density, and concomitantly an increase in average void size. Soft

impingement seems to take place at ≥0.2 dpa where the void size experiences a more rapid increase with the damage level. The presence of only 5wt.%Ta in solid solution hinders the diffusion of free radiation-induced vacancies at 800 °C, and consequently precludes the formation of voids up to 0.3 dpa. Moreover, solute Ta atoms also induce a remarkable increase in void density at 1000 °C as compared to W under equivalent irradiation conditions, and a gradual progression in average void size towards saturation at ≥0.2 dpa. Furthermore, a significant number of voids in both materials, initially formed as spherical embryos, experience a progressive transition to a faceted shape at ≥0.3 dpa.

Acknowledgments

The authors of this work acknowledge access to the MIAMI-II facility through the EPSRC-funded mid-range facility, the UK National Ion Beam Centre (NS/A000059/1). In addition, access to sample preparation equipment provided by the Dalton Cumbrian Facility of The University of Manchester is acknowledged. Authors I.I., M.J.D.R. and S.C.M. are supported through the Sêr Cymru Nuclear Futures Institute funded through WEFO (Wales). We would particularly like to thank Prof. W.E. Lee for his support and guidance.

References

[1] D. Hancock, D. Homfray, M. Porton, I. Todd, B. Wynne, Refractory metals as structural materials for fusion high heat flux components. J. Nucl. Mater. 512 (2018) 169-183.

[2] T. Hirai, S. Panayotis, V. Barabash, C. Amzallag, F. Escourbiac, A. Durocher et al., Use of tungsten material for the ITER divertor. Nucl. Mater. Energy 9 (2016) 616–22.

[3] M. Rieth, S.L. Dudarev, S.M. Gonzalez de Vicente, J. Aktaa, T. Ahlgren, S. Antusch, et al., Recent progress in research on tungsten materials for nuclear fusion applications in Europe. J. Nucl. Mater. 432 (2013) 482-500.

[4] S.J. Zinkle, A. Mösslang, T. Muroga, H. Tanigawa, Multimodal options for materials research to advance the basis for fusion energy in the ITER era. Nucl. Fusion 53 (2013) 104024 (13pp).

[5] R.G. Abernethy, Predicting the performance of tungsten in a fusion environment: a literature review, Mater. Sci. Technol. 33 (2017) 388.

[6] C. Thomser, V. Bailescu, S. Brezinsek, J.W. Coenen, H. Greuner, T. Hirai et al., Plasma Facing Materials for the JET ITER-Like Wall. Fusion Sci. Technol. 62 (2012) 1–8.

[7] A. Widdowson, E. Alves, A. Baron-Wiechec, N.P. Barradas, N. Catarino, J.P. Coad et al., Overview of the JET ITER-like wall divertor. Nucl. Mater. Energy 12 (2017) 499–505.

[8] R. Villari, V. Barabash, F. Escourbiac, L. Ferrand, T. Hirai, V. Komarov et al., Nuclear analysis of the ITER full-tungsten divertor. Fusion Eng. Des. 88 (2013) 2006–10.

[9] S.Heuer, Th.Weber, G.Pintsuk, J.W.Coenen, J.Matejicek, Ch.Linsmeier, Aiming at understanding thermo-mechanical loads in the first wall of DEMO: Stress–strain evolution in a Eurofer-tungsten test component featuring a functionally graded interlayer. Fus. Eng. Design 135 (2018) 141-153.

[10] A. Li-Puma, M. Richou, P. Magaud, M. Missirlian, E. Visca, V.P. Ridolfini, Potential and limits of water cooled divertor concepts based on monoblock design as possible candidates for a DEMO reactor. Fusion Eng. Des. 88 (2013) 1836-1843.

[11] S.J. Zinkle, N.M. Ghoniem, Operating temperature windows for fusion reactor structural materials. Fusion Eng. Des. 51-52 (2000) 55-71.

[12] T. Shen,Y. Dai,Y. Lee, Microstructure and tensile properties of tungsten at elevated temperatures. J. Nucl. Mater. 468 (2016) 348-354.

[13] P. Gumbsch. Brittle fracture and the brittle-to-ductile transition of tungsten, J. Nucl. Mater. 323 (2003) 304-312.

[14] B.Gludovatz, S.Wurster, A.Hoffmann, R.Pippan, Fracture toughness of polycrystalline tungsten alloys. Int. J. Refract. Met. Hard Mater. 28 (2010) 674-678.

[15] E. Gaganidze, D. Rupp, J. Aktaa, Fracture behaviour of polycrystalline tungsten. J. Nucl. Mater. 446 (2014) 240-245.

[16] H. Bolt, V. Barabash, G. Federici, J. Linke, A. Loarte, J. Roth, K. Sato, Plasma facing and high heat flux materials – needs for ITER and beyond. J. Nucl. Mater. 307-311 (2002) 43-52.

[17] I.V. Gorynin, V.A. Ignatov, V.V. Rybin, S.A. Fabritsiev, V.A. Kazakov, V.P. Chakin, et al., Effects of neutron irradiation on properties of refractory metals. J. Nucl. Mater. 191-194 (1992) 421-425.

[18] L.K. Keys, J.P. Smith, J. Moteff, Stage III recovery in neutron irradiated tungsten. Scripta Metall. 1 (1967) 71-72.

[19] V.K. Sikka, J. Moteff, “Rafting” in neutron irradiated tungsten. J. Nucl. Mater. 46 (1973) 217-219.

[20] T. Koyanagi, N.A.P. Kiran Kumar, T. Hwang, L.M. Garrison, X. Hu, L.L. Snead, Y. Katoh, Microstructural evolution of pure tungsten neutron irradiated with a mixed energy spectrum. J. Nucl. Mater. 490 (2017) 66-74.

[21] J.M. Galligan, T. Oku, Dislocation Loops in Neutron Irradiated Tungsten. Phys. Stat. Sol. 36 (1969) K79-K82.

[22] T. Koyagani, N.A.P. Kiran Kumar, T. Hwang, L.M. Garrison, X. Hu, L.L. Snead, Y. Katoh. Microstructural evolution of pure tungsten neutron irradiated with a mixed energy spectrum. J. Nucl. Mater. 490 (2017) 66-74.

[23] X. Hu, T. Koyanagi, M. Fukuda, N.P.P. Kiran Kumar, L.L. Snead, B.D. Wirth, Y. Katoh, Irradiation hardening of pure tungsten exposed to neutron irradiation. J. Nucl. Mater. 480 (2016) 235-243.

[24] X. Hu, C.M. Parish, K. Wang, T. Koyamagi, B.P. Eftink, Y. Katoh, Transmutation-induced precipitation in tungsten irradiated with a mixed energy spectrum. Acta Mater. 165 (2019) 51-61.

[25] R.W. Harrison, On the use of ion beams to emulate the neutron irradiation behaviour of tungsten. Vacuum 160 (2019) 355-370.

[26] X. Yi, M.L. Jenkins, M. Briceno, S.G. Roberts, Z. Zhou, M.A. Kirk, *In-situ* study of self-ion irradiation damage in W and W-5Re at 500°C. Phil. Mag. 93 (2013) 1715-1738.

[27] F. Ferroni, X. Yi, K. Arakawa, S.P. Fitzgerald, P.D. Edmonson, S.G. Roberts, High temperature annealing of ion irradiated tungsten. Acta Mater. 90 (2015) 380-393.

[28] M. Rieth, S.L. Dudarev, S.M. Gonzalez de Vicente, J.Aktaa, T.Ahlgren, S.Antusch, et al., A brief summary of the progress on the EFDA tungsten materials program. J. Nucl. Mater. 442 (2013) S173-S180.

[29] D. Jiang, Q. Wang, W. Hu, Z. Wei, J. Tong, H. Wan, The effect of tantalum (Ta) doping on mechanical properties of tungsten (W): A first-principles study. J. Mater. Res. 31 (2016) 3401-3408.

[30] Z. Wang, Y. Yuan, K. Arshad, J. Wang, Z. Zhou, J. Tang, G.-H. Lu, Effects of tantalum concentration on the microstructures and mechanical properties of tungsten-tantalum alloys. Fusion Eng. Des. 125 (2017) 496-502.

[31] P.E.A. Turchi, A. Gonis, V. Drchal, J. Kudmonvský, First-principles study of stability and local order in substitutional Ta-W alloys. Phys. Rev. B 64 (2001) 085112 (8pp).

[32] D.E.J. Armstrong, A.J. Wilkinson, S.G. Roberts, Mechanical properties of ion-implanted tungsten-5wt,% tantalum. Phys. Scr. T145 (2011) 014076 (4pp).

[33] X. Yi, M.L. Jenkins, K. Hattar, P.D. Edmondson, S.G. Roberts, Characterisation of radiation damage in W and W-based alloys from 2 MeV self-ion near-bulk implantations. Acta Mater. 92 (2015) 163-177.

[34] A. Xu, D.E.J. Armstrong, C. Beck, M.P. Moody, G.D.W. Smith, P.A.J. Bagot et al., Ion-irradiation induced clustering in W-Re-Ta, W-Re and W-Ta alloys: An atom probe tomography and nanoindentation study. Acta Mater. 124 (2017) 71-78.

[35] I. Ipatova, R.W. Harrison, P.T. Wady, S.M. Shubeita, D. Terentyev, S.E. Donnelly, E. Jimenez-Melero, Structural defect accumulation in tungsten and tungsten-5wt,% tantalum under incremental proton damage. J. Nucl. Mater. 501 (2017) 329.

[36] W. Setyawan, G. Nandipati, R.J. Kurtz, Ab initio study of interstitial cluster interaction with Re, Os, and Ta in W. J. Nucl. Mater. 484 (2017) 30-41

[37] L.K. Keys, J.Moteff, Neutron irradiation and defect recovery of tungsten. J. Nucl. Mater. 34 (1970) 260-280.

[38] Y.-W. Kim, J.M. Galligan, An annealing study of thermal neutron irradiated tungsten. J. Nucl. Mater. 69 & 70 (1978) 680-682.

[39] D.N. Seidman, On the point-defect annealing mechanism for stage III recovery in irradiated or quenched tungsten. Scripta Metall. 13 (1979) 251-257.

[40] T. Tanno, M. Fukuda, S. Nogami, A. Hasegawa. Microstructure Development in Neutron Irradiated Tungsten Alloys. Mater. Trans. 52 (2011) 1447-1451.

[41] I. Ipatova, R.W. Harrison, D. Terentyev, S.E. Donnelly, E. Jimenez-Melero, Thermal evolution of the proton irradiated structure in tungsten-5wt% tantalum, J. Fusion Energy 36 (2017) 234-239.

[42] X. Yi, K. Arakawa, Y. Du, F. Ferroni, W. Han, P. Liu, F. Wan, High-temperature defect recovery in self-ion irradiated W-5 wt% Ta. Nucl. Mater. Energy 18 (2019) 93–98.

[43] M.R. Gilbert, S.L. Dudarev, P.M. Derlet, D.G. Pettifor, Structure and metastability of mesoscopic vacancy and interstitial loop defects in iron and tungsten. J. Phys.: Condens. Matter 20 (2008) 345214 (10pp).

[44] J. Matolich H. Nahm, J. Moteff, Swelling in neutron irradiated tungsten and tungsten-25 percent rhenium. Scripta Metall. 8 (1974) 837-841.

[45] V.K. Sikka, J. Moteff, Superlattice of voids in neutron-irradiated tungsten. J. Appl. Phys. 43 (1972) 4942-4944.

[46] J. Linke, T. Loewenhoff, V. Massaut, G. Pintsuk, G. Ritz, M. R€odig, A. Schmidt, C. Thomser, I. Uytdenhouwen, V. Vasechko, M. Wirtz, Performance of different tungsten grades under transient thermal loads. Nucl. Fusion 51 (2011) 073017.

[47] Y. Zayachuk, M.H.J. t Hoen, P.A. Zeijlmans van Emmichoven, D. Terentyev, I. Uytdenhouwen, G. van Oost, Nucl., Surface modification of tungsten and tungsten–tantalum alloys exposed to high-flux deuterium plasma and its impact on deuterium retention. Fusion 53 (2013) 013013.

[48] J.A. Hinks, J.A. van den Berg, S.E. Donnelly. MIAMI: Microscope and ion accelerator for materials investigations. J. Vac. Sci. Technol. A-Vac. Surf. Films 29 (2011) 021003 (6pp).

[49] J.F. Ziegler, Stopping of energetic light ions in elemental matter. J. Appl. Phys. 85 (1999) 1249-1272.

[50] J.F. Ziegler, M.D. Ziegler, J.P. Biersack, SRIM – The stopping and range of ions in matter (2010). Nucl. Instrum. Meth. Phys. Res. B 268 (2010) 1818-1823.

[51] ASTM E521-96, Standard Practice for Neutron Radiation Damage Simulation by Charged-particle Irradiation, 2009.

[52] M.L. Jenkins, M.A. Kirk, Characterization of Radiation Damage by Transmission Electron Microscopy, IOP Publishing Ltd, 2001.

[53] B.N. Singh, On the influence of grain boundaries on void growth. Phil. Mag. 28 (1973) 1409-1413.

[54] D.I.R. Norris, The use of the high voltage electron microscope to simulate fast neutron-induced void swelling in metals. J. Nucl. Mater. 40 (1971) 66.

[55] K.W. Ingle, A.G. Crocker, The interaction between vacancies and $\frac{1}{2}$ <111> {1-10} edge dislocation in body centred cubic metals. Acta Metall. 26 (1978) 1461-1469.

[56] B.L. Eyre, D.M. Maher, Neutron irradiation damage in molybdenum. Philos. Mag. 24 (1971) 767-797.

[57] X.-S. Kong, X. Wu, Y.-W. You, C.S. Liu, Q.F. Fang, J.-L. Chen et al., First-principles calculations of transition metal–solute interactions with point defects in tungsten. Acta Mater. 66 (2014) 172-183.

[58] F.A. Smidt Jr., J.A. Sprague, Suppression of void nucleation by a vacancy trapping mechanism. Scripta Metall. 7 (1973) 495-501.

[59] W.B. Liu, N. Wang, Y.Z. Ji, P.C. Song, C. Zhang, Z.G. Yang et al., Effects of surface energy anisotropy on void evolution during irradiation: A phase-field model. J. Nucl. Mater. 479 (2016) 316-322.

Tables

Table 1. The main experimental parameters that characterise the in-situ proton irradiation of W and W-5Ta materials at 800 °C and 1000 °C. The samples were studied in-situ by TEM at selected incremental damage levels. The fluence given in the table refers to the total value achieved at the end of the irradiation. The damage level corresponds to the average value over the disc thickness of ~100–110 nm studied by in-situ TEM.

Table 2. The main parameters that characterise the population of radiation-induced voids observed in W and W-5Ta materials at selected damage levels.

Figure captions

Fig. 1. Electron Backscattered Diffraction maps of the W and W-5Ta microstructures prior to proton irradiation (taken from [35]).

Fig. 2. In-situ observation of void growth, together with changes in void shape (insets), in W under increasing damage levels induced by a 40 keV proton beam at 800 °C and 1000°C. Yellow dotted line denotes denuded zone.

Fig. 3. In-situ observation of void growth, together with changes in void shape (insets) in W-5Ta material under increasing damage levels induced by 40 keV proton bombardment at 1000°C. Radiation-induced voids were not detected in the irradiated material at 800 °C, but can be seen in the same sample after post-irradiation annealing at 1000 °C.

Fig. 4. Average size and number-density of voids in W and W-5Ta alloy as a function of damage level, at the irradiation temperature of either 800 or 1000 °C. Voids were not detected in the W-5Ta proton irradiated up to a damage level of 0.3dpa at 800 °C.

Fig. 5. Void agglomeration and change in void shape in W-5Ta at selected damage levels, induced by 40 keV proton bombardment at 1000 °C.

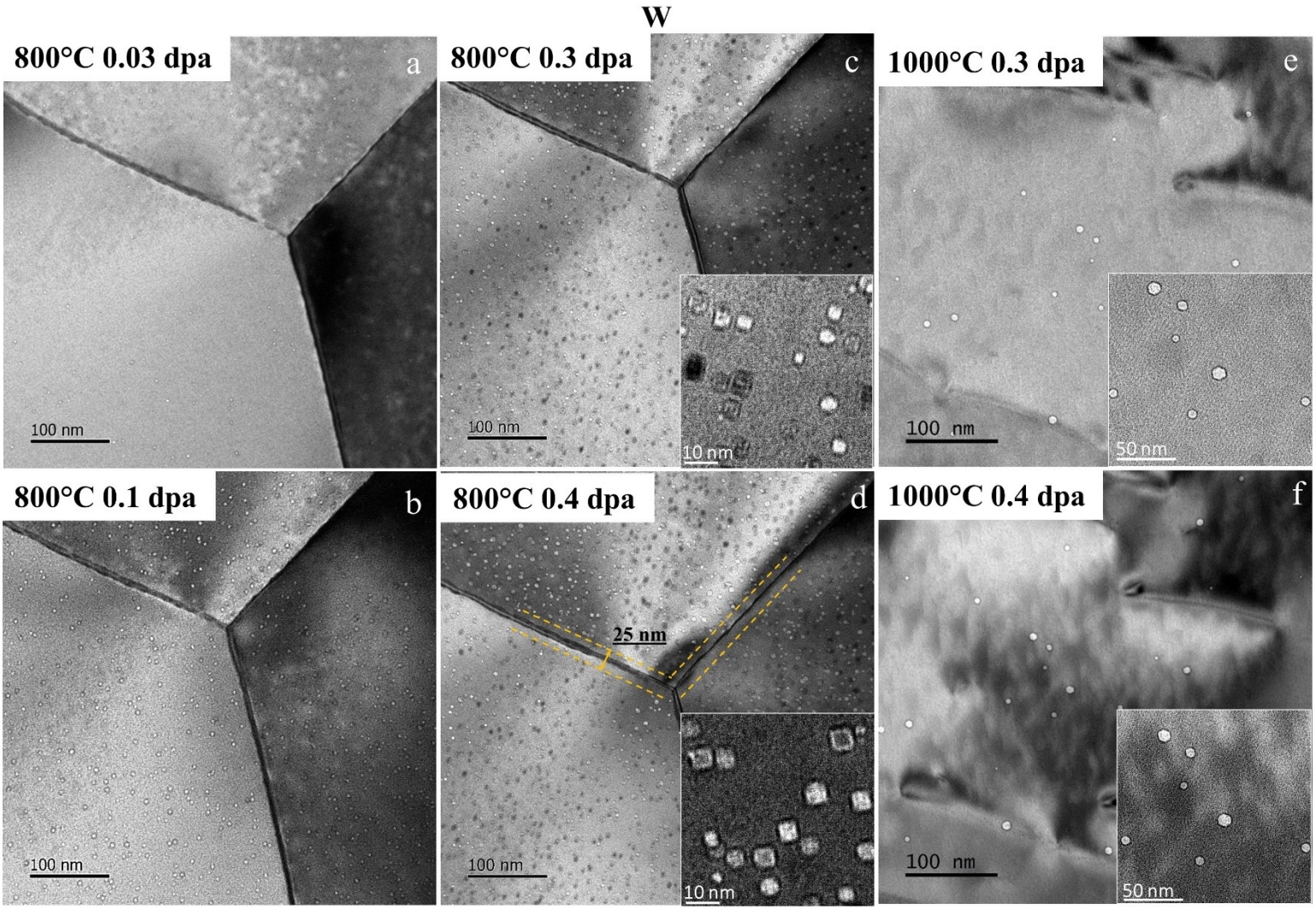

Fig. 1. In-situ observation of void growth, together with changes in void shape (insets), in **W** under increasing damage levels induced by a 40 keV proton beam at 800 °C: (a) 0.03 dpa, (b) 0.1dpa, (c) 0.3 dpa, (d) 0.4 dpa; and 1000°C: (e) 0.3 dpa, (f) 0.4 dpa. Yellow dotted line denotes denuded zone.

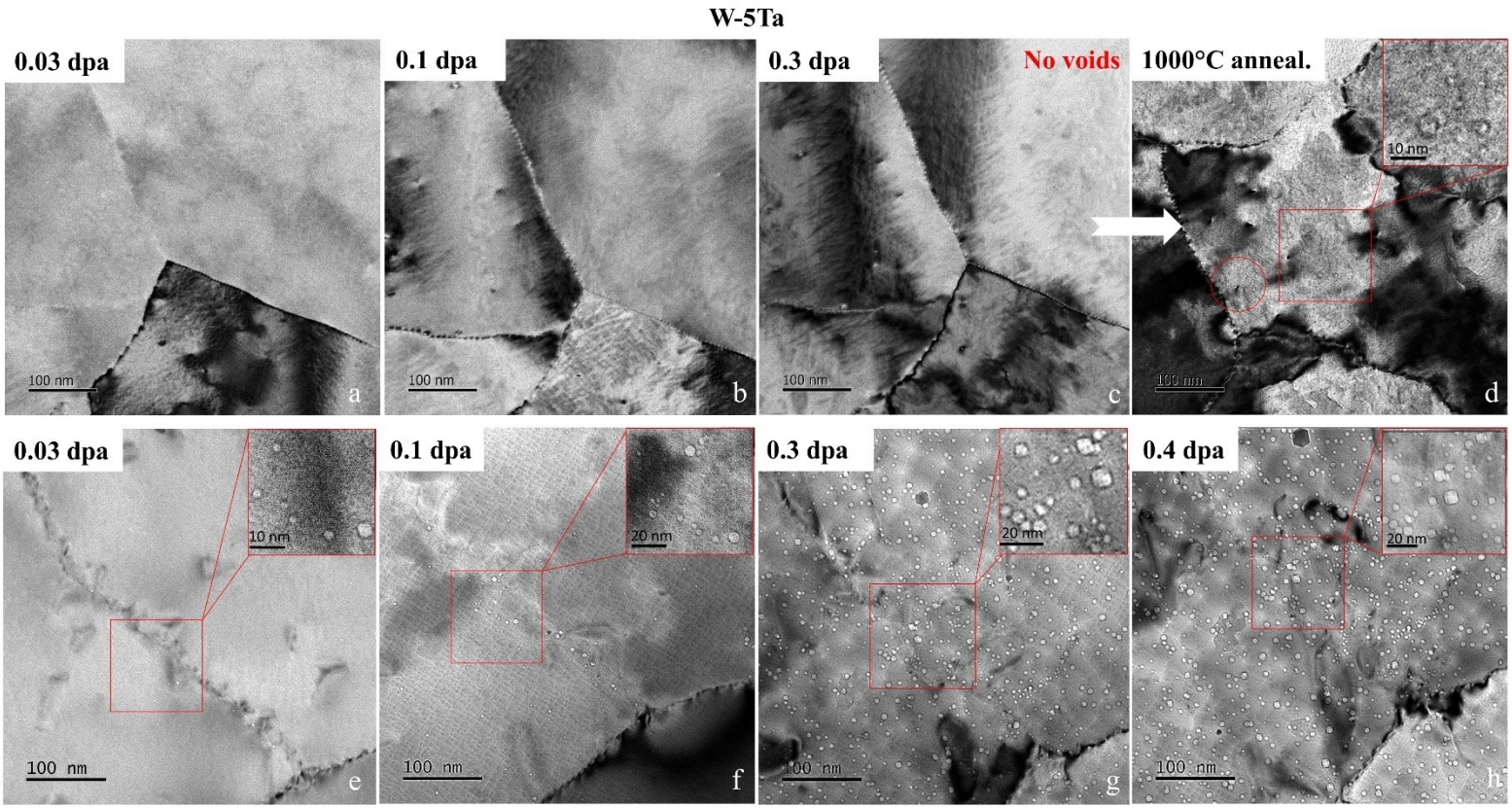

Fig. 2. In-situ observation of void growth, together with changes in void shape (insets) in **W-5Ta** under increasing damage levels induced by 40 keV proton bombardment at 800 °C: (a) 0.03 dpa, (b) 0.1dpa, (c) 0.3 dpa, (d) after post-irradiation annealing at 1000°C; and 1000°C at 800 °C: (e) 0.03 dpa, (f) 0.1dpa, (g) 0.3 dpa, (h) 0.4 dpa. Radiation-induced voids were not detected in the irradiated material at 800 °C, but can be seen in the same sample after post-irradiation annealing at 1000 °C.

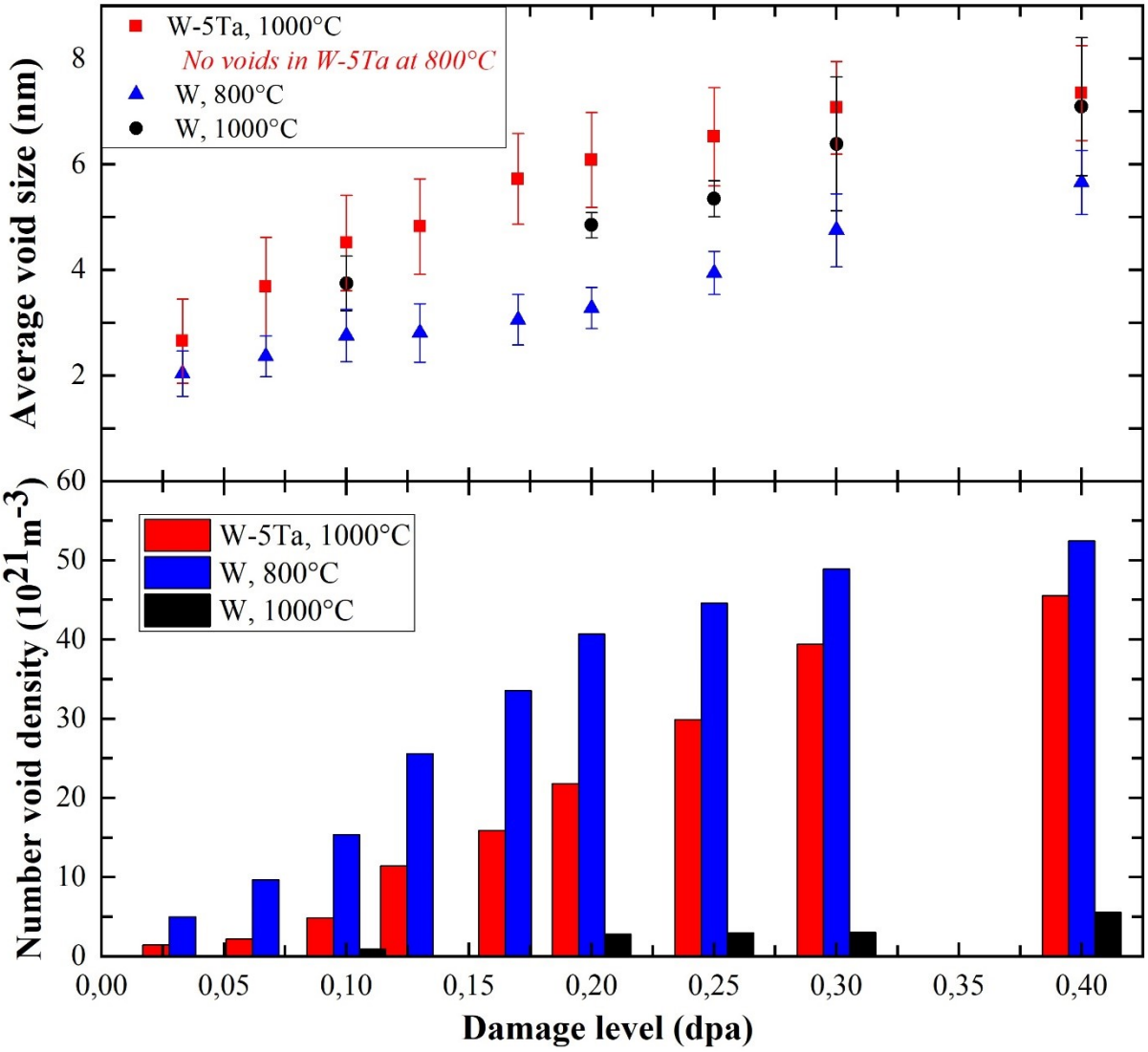

Fig. 3. Average size and number-density of voids in **W** and **W-5Ta** alloy as a function of damage level, at the irradiation temperature of either 800 or 1000 °C. Voids were not detected in the W-5Ta proton irradiated up to a damage level of 0.3dpa at 800 °C.

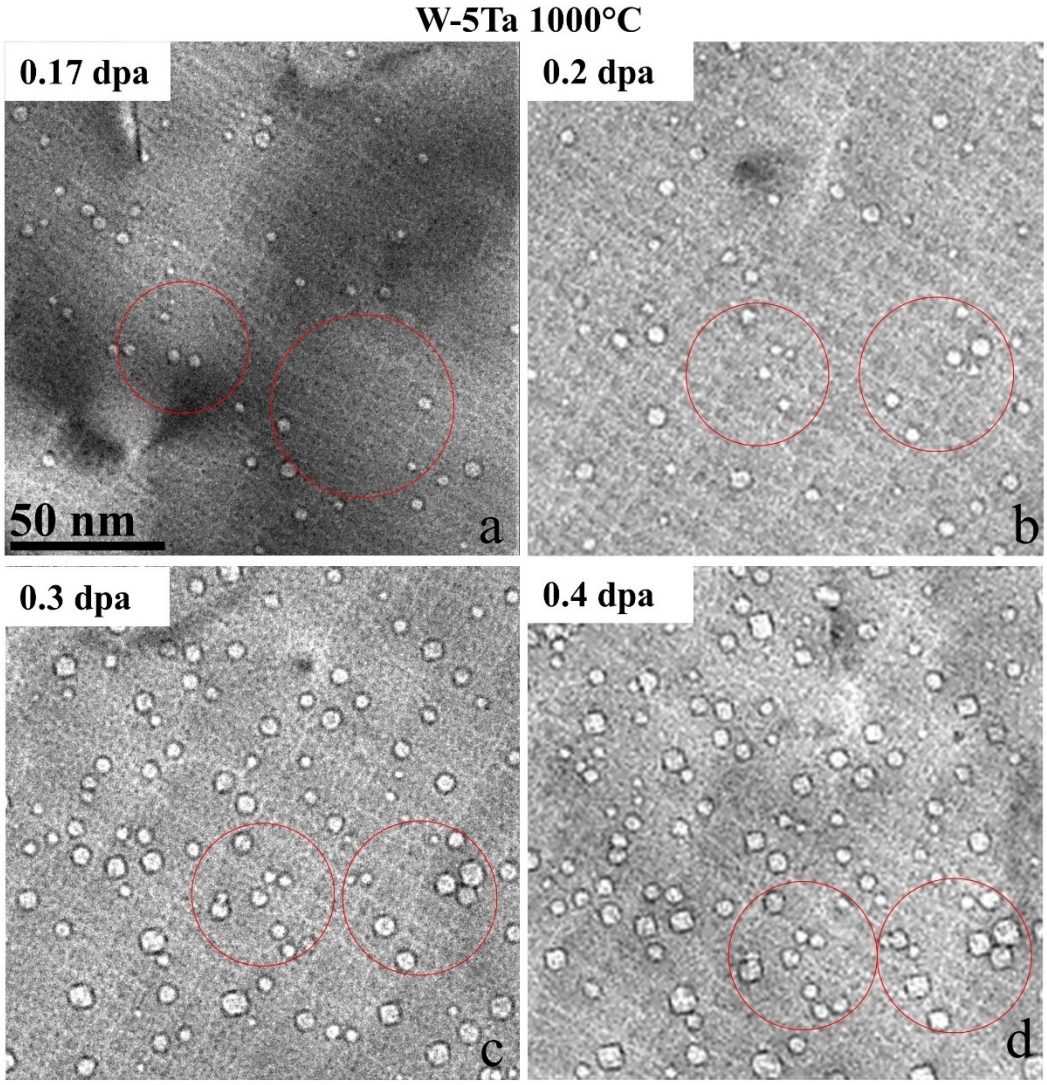

Fig. 4. Void agglomeration and change in void shape in **W-5Ta** at selected damage levels, induced by 40 keV proton bombardment at 1000 °C: (a) 0.17 dpa, (b) 0.2 dpa, (c) 0.3 dpa, (d) 0.4 dpa.

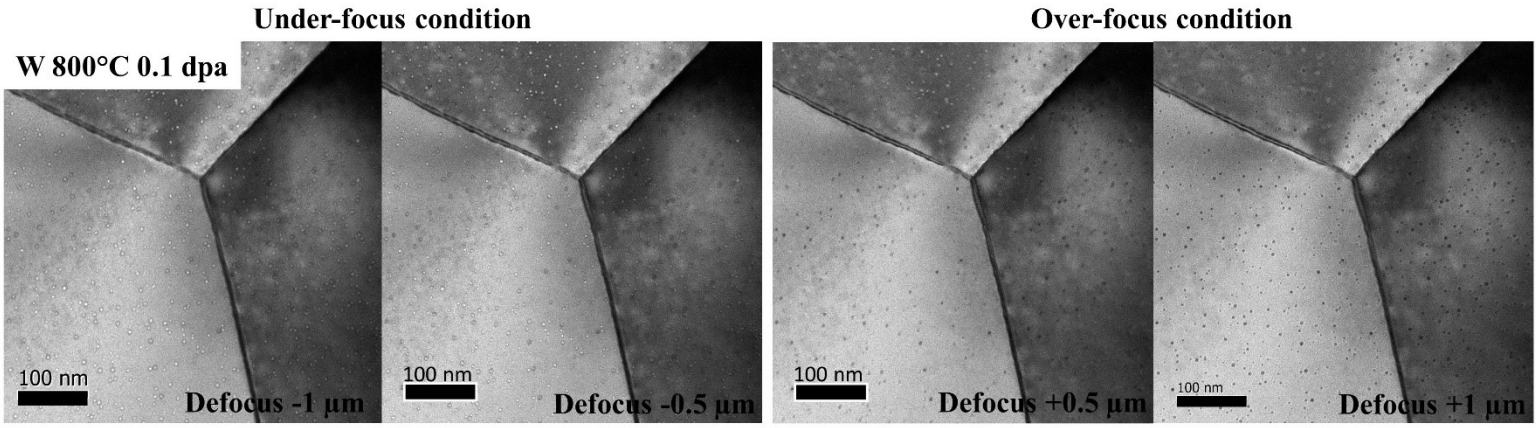

Fig. S1. Bright field TEM imaging of radiation-induced voids in **W** at the temperature of 800 °C and the damage level of 0.1 dpa, based on the out-of-focus imaging technique with selected defocus values up to +/-1 µm.

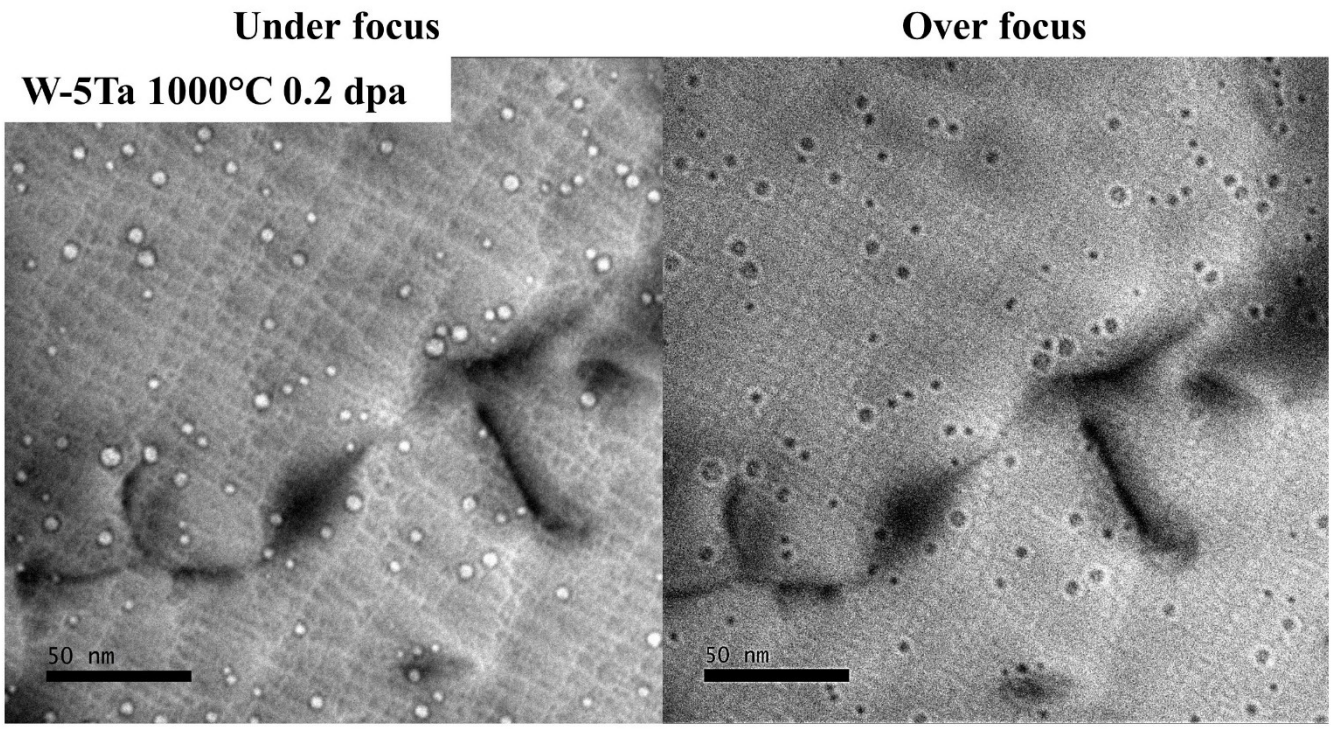

Fig. S2. Bright field TEM images of voids in **W-5Ta** proton-irradiated at 1000 °C and to a damage level of at 0.2 dpa. The images were taken using the out-of-focus imaging technique with the defocus value of +/-500 nm. Dislocations present in the micrographs correspond to pre-existing dislocations prior to irradiation.

Table 1

Temperature (°C)	**800°C**		**1000°C**	
Material	**W**	**W-Ta**	**W**	**W-Ta**
Proton energy	40 keV			
Current (nA)	0.29	0.15	0.17	0.2
Fluence (ions/cm^2)	7.66×10^{17}	4.7×10^{17}	7.66×10^{17}	6.3×10^{17}
Flux (ions/cm^2/s)	1.15×10^{14}	6×10^{13}	6.8×10^{13}	8×10^{13}
Damage rate (dpa/s)	7.3×10^{-5}	3.8×10^{-5}	4.3×10^{-5}	5.05×10^{-5}
Damage level (dpa)	0.5	0.3	0.5	0.4

Table 2

Material	Temperature, °C	Damage level, dpa	Average void size, nm	Void density, $10^{21} m^{-3}$	Fraction of squared voids at 0.4 dpa*, %
W	**800°C**	**0.2**	3.3 ± 0.4	40.7± 4.1	
		0.4	5.7 ± 0.6	52.5 ± 5.3	
	1000°C	**0.2**	4.9 ± 0.3	2.8 ± 0.3	
		0.4	7.1 ± 1.3	5.6 ± 0.6	30
W-5Ta	**800°C** ↓	*No voids observed*			
	Annealed at 1000°C	**after 0.3**	4.86 ± 1.4	1.4 ± 0.1	
	1000°C	**0.2**	6.1 ± 0.9	21.8 ± 2.2	
		0.4	7.4 ± 0.9	45.5 ± 4.6	12

* The fraction of square voids was calculated at the maximum damage level (0.4 dpa) for W sample irradiated at 800°C and W-5Ta sample irradiated at 1000°C due to the highest density of the voids.